Journal of Scientific Computing, Vol. 17, Nos. 1–4, December 2002 (© 2002)

Numerical Entropy Production on Shocks and Smooth Transitions

Gabriella Puppo[1]

Received July 24, 2001; accepted (in revised form) October 31, 2001

In this work, we propose an algorithm to measure the numerical entropy production of several high order central schemes. The results obtained on a numerical test indicate that this quantity permits to estimate the local error, in regions of smooth flow, and to detect and locate shocks.

KEY WORDS: Conservation laws; numerical entropy; central difference schemes; high-order accuracy; a posteriori error.

1. INTRODUCTION

In this work, we describe the behaviour of the numerical cell entropy production for several schemes. The numerical results we show indicate that numerical entropy production can be used to estimate the local error in regions of smoothness and to locate shocks. Thus the numerical entropy production can be computed at each time step to monitor the numerical solution produced by a scheme. The information gained in this fashion can be used in strategies of grid adaptivity and/or to enhance the resolution of discontinuities. We also describe how, at least for central schemes, the evaluation of numerical entropy production does not result in a substantial extra computational cost.

We consider the one-dimensional system of conservation laws:

$$u_t + f_x(u) = 0 \tag{1.1}$$

endowed with an entropy function $\eta(u)$ which satisfies the entropy inequality:

$$\eta_t + \psi_x \leqslant 0, \qquad \text{with} \quad \nabla_u^T \psi = \nabla_u^T \eta(u)\, f'(u) \tag{1.2}$$

[1] Dipartimento di Matematica, Politecnico di Torino, Corso Duca degli Abruzzi 24, 10129 Torino, Italy. E-mail: puppo@calvino.polito.it

0885-7474/02/1200-0263/0 © 2002 Plenum Publishing Corporation

where $f'(u)$ is the Jacobian of f. We cover the computational region with control volumes $V_j^n = I_j \times [t^n, t^{n+1}]$, where $t^{n+1} = t^n + \Delta t$, $I_j = [x_j - h/2, x_j + h/2]$ and $x_{j+1} = x_j + h$.

Integrating the conservation laws (1.1) over the control volumes V_j^n, we find the finite volume formulation:

$$\bar{u}_j^{n+1} = \bar{u}_j^n - \frac{1}{h} \int_{t^n}^{t^{n+1}} [f(u(I_j^+, \tau)) - f(u(I_j^-, \tau))]\, d\tau \tag{1.3}$$

Here I_j^+ and I_j^- denote the right and left end points of the interval I_j and $\bar{u}_j^n = \frac{1}{h} \int_{I_j} u(x, t^n)$ is the cell average at time $t^n = n\,\Delta t$. Finally, $\lambda = \Delta t / h$ will denote the mesh ratio.

Integrating the entropy inequality over the same control volume, we find the finite volume formulation of the entropy inequality:

$$\bar{\eta}_j^{n+1} - \bar{\eta}_j^n + \frac{1}{h} \int_{t^n}^{t^{n+1}} [\psi(u(I_j^+, \tau)) - \psi(u(I_j^-, \tau))]\, d\tau \leqslant 0 \tag{1.4}$$

where $\bar{\eta}_j^n$ is the cell average of the function $\eta(u(x, t))$ in the cell I_j at time t^n. In smooth regions, equality holds, both in (1.3) and (1.4). If a shock crosses the V_j^n control volume, (1.3) is satisfied, but (1.4) will not be zero, instead its sign characterizes the physically relevant unique solution to (1.1).

In finite volume schemes the updated cell averages at time t^{n+1} are computed through a discretization of (1.3). However the discretized version of the entropy inequality will not be zero, even on smooth flows.

Let:

$$S_j^n = \frac{1}{\Delta t} \left\{ \bar{\eta}_j^{n+1} - \bar{\eta}_j^n + \frac{1}{h} \int_{t^n}^{t^{n+1}} [\psi(u)|_{I_j^+} - \psi(u)|_{I_j^-}]\, d\tau \right\} \tag{1.5}$$

be the density of numerical entropy production in the V_j^n control volume (in the following it will be called entropy production, for short, when no ambiguities arise). Here u denotes the computed numerical solution of the finite volume scheme.

Central schemes based on staggered grids yield a natural way for the evaluation of S_j^n. In fact in these schemes the solution is smooth on the walls of control volumes, see for instance [4]. This enables the evaluation of the time integrals of the entropy fluxes, using data already computed in order to find $\bar{u}^{n+1}$.

In this work, we continue the study we started in [5]. We compute the entropy production on a gas dynamic test problem for several central schemes. The test chosen was described in [6]. It consists of the interaction of a Mach 3 shock with an acoustic wave. The numerical solution has a very rich structure, which better shows the advantages of high order schemes.

We will see that the numerical entropy production indeed signals the presence of discontinuities in the solution. Moreover, in regions of smooth flow, the spurious numerical entropy production mimics the behaviour of the local error.

In the following section, we review the construction of central schemes based on staggered grids. Next we define the numerical entropy production for these schemes. In the last section, we compare the numerical entropy production of several schemes with the behaviour of the corresponding numerical solutions.

The schemes studied in this work are the second order Nessyahu–Tadmor scheme (NT) described in [4], the third order Compact Central WENO (C-CW3) scheme of [3] and the fourth order Central WENO (CW4) method introduced in [2].

2. ENTROPY PRODUCTION FOR CENTRAL SCHEMES

Central schemes are based on the integration of the conservation law (1.1) on staggered cells. More precisely, starting from the cell averages $\{\bar{u}_j^n\}$ at time t^n, we reconstruct the initial data:

$$u^n(x) = \sum_j P_j(x)\, \chi_{I_j}(x) \tag{2.1}$$

where $P_j(x)$ is a non-oscillatory polynomial, interpolating the numerical solution in the sense of cell averages, to ensure conservation, and χ_{I_j} is the characteristic function of the interval I_j. For the NT scheme, the reconstruction is piece-wise linear, while for C-CW3 and CW4 schemes it is piecewise parabolic. See the references for the details of the algorithms defining the reconstruction.

Once the reconstruction has been computed, the conservation law is enforced on the staggered control volume $V_{j+1/2}^n = [x_j, x_{j+1}] \times [t^n, t^{n+1}]$. Thus the interaction of the discontinuities in the initial data $u^n(x)$ lie in the middle of the control volumes. Therefore, the solution of the conservation law remains smooth at the walls $\{x_j\} \times [t^n, t^{n+1}]$ and $\{x_{j+1}\} \times [t^n, t^{n+1}]$ of the staggered control volume, if Δt is small enough, and the time integrals of the fluxes appearing in (1.3) can be approximated by quadrature:

$$\int_{t^n}^{t^{n+1}} f(u(x_j, \tau))\, d\tau \simeq \Delta t \sum_{l=0}^{M} w_l f(u(x_j, t^n + \tau_l)) \tag{2.2}$$

The midpoint rule, $M = 0$, $w_0 = 1$, $\tau_0 = \frac{\Delta t}{2}$, is enough for second order accuracy, and it is used for the NT scheme. Simpson's rule is used for the C-CW3 and CW4 schemes: $M = 2$, $w_0 = w_2 = \frac{1}{6}$, $w_1 = \frac{2}{3}$, and $\tau_0 = 0$, $\tau_1 = \frac{\Delta t}{2}$, $\tau_2 = \Delta t$.

The values of $u(x_j, t^n + \tau_l)$ can be easily predicted using the local smoothness of the numerical solution. For the NT scheme:

$$u\left(x_j, t^n + \frac{\Delta t}{2}\right) := u(x_j, t^n) - \frac{\Delta t}{2} f'(u(x_j, t^n))\, u_x(x_j, t^n)$$

where f' is the Jacobian of f and $u(x_j, t^n)$ and $u_x(x_j, t^n)$ are computed via the reconstruction (2.1).

For the C-CW3 and the CW4 schemes, the values of $u(x_j, t^n+\tau_l)$ are evaluated applying a Runge–Kutta method to the system of equations $u_t|_{x_j} = -f_x(u)|_{x_j}$. This again involves reconstruction steps to interpolate the data $f(u(x_j, .))$, in order to estimate $f_x(u)|_{x_j}$.

The density of numerical entropy production can be defined as:

$$S_{j+1/2} = \frac{1}{\Delta t}\left\{\bar{\eta}^{n+1}_{j+1/2} - \bar{\eta}^{n}_{j+1/2} + \lambda \sum_l w_l(\psi(u(x_{j+1}, t^n+\tau_l) - \psi(u(x_j, t^n+\tau_l))\right\} \tag{2.3}$$

Here the averages of the entropies are given by:

$$\bar{\eta}^{n}_{j+1/2} = \frac{1}{h}\int_{x_j}^{x_{j+1}} \eta(u^n(x))\, dx \tag{2.4}$$

For the evaluation of $\bar{\eta}^{n+1}_{j+1/2}$ it is necessary to anticipate the reconstruction step on the updated cell averages at the end of the previous time step. Thus, the integral in (2.4) can be approximated both at $t = t^n$ and $t = t^{n+1}$ by quadrature. Note that all quantities involved in the computation of $S_{j+1/2}$ in (2.3) must be computed to update the cell averages of the numerical solution. Thus the evaluation of the entropy production does not add a substantial overhead to the computation of the time advancement of the solution.

3. NUMERICAL RESULTS

We are considering the one-dimensional Euler's equations for an ideal gas. The vector of unknowns is $u = (\rho, \rho v, \frac{1}{2}\rho v^2 + \rho e)^T$, where ρ is the density, v is the velocity and e is the internal energy, linked to the pressure p by the equation of state $p = \rho e(\gamma - 1)$, with $\gamma = 1.4$. The entropy is $\eta = -\rho \log(\rho e/\rho^\gamma)$, and the entropy flux is $\psi = v\eta$, see [1].

The test we are studying is due to Shu and Osher, [6]. It consists of a Mach 3 shock interacting with an acoustic wave. The initial condition is $u = u_L$ for $x \leqslant 0.1$, and $u = u_R$ for $x > 0.1$. The computational domain is $[0, 1]$, with free-flow boundary conditions. The left (L) and right (R) states are given by:

$$\begin{pmatrix} \rho \\ v \\ p \end{pmatrix}_L = \begin{pmatrix} 3.857143 \\ 2.629369 \\ 10.3333 \end{pmatrix} \qquad \begin{pmatrix} \rho \\ v \\ p \end{pmatrix}_R = \begin{pmatrix} 1+0.2\sin(50x) \\ 0 \\ 1 \end{pmatrix}$$

The Courant number for this flow is $c \simeq 0.219$. The solution is printed at $T = 0.18$.

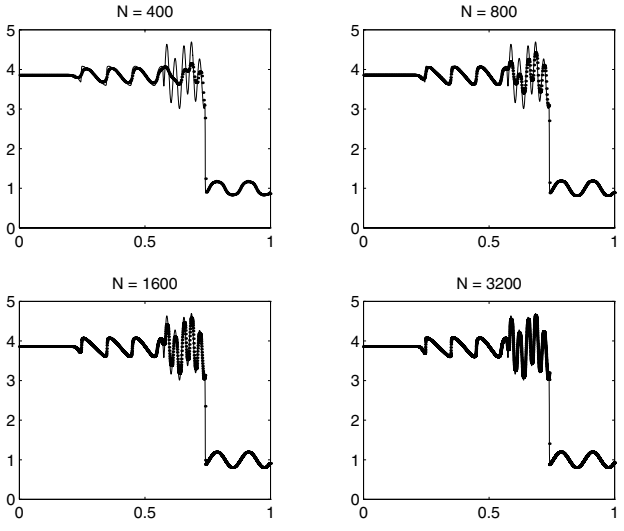

Fig. 1. NT scheme: density; $\lambda = 0.45c$.

In this test, the acoustic wave is filtered by the shock. A region of smooth flow with a complex structure occurs right behind the shock. A series of weak waves emerges from this smooth region; these waves steepen into shocks as they move away from the shock. At $T = 0.18$, two shocks have already formed behind the initial Mach 3 shock, trailed by a third wave, which has not yet steepened into a shock.

In the following figures, the numerical solution is drawn with a dotted line, and the solid line denotes the "*exact*" solution, which was obtained running the CW4 scheme with a grid of 1600 points. Finally, N is the number of grid points.

We want to focus on two topics:

- the behaviour of the entropy production in the region of smooth flow behind the main shock;
- the behaviour of the entropy production on shocks.

Figure 1 shows the density obtained with the NT scheme at $T = 0.18$ for several grid sizes. The numerical solutions due to the C-CW3 and CW4 schemes can be found in Figs. 4 and 6 respectively.

The corresponding plots for the density of entropy production behind the main shock appear in Fig. 2 (NT scheme), Fig. 5 (C-CW3 scheme) and Fig. 7 (CW4 scheme).

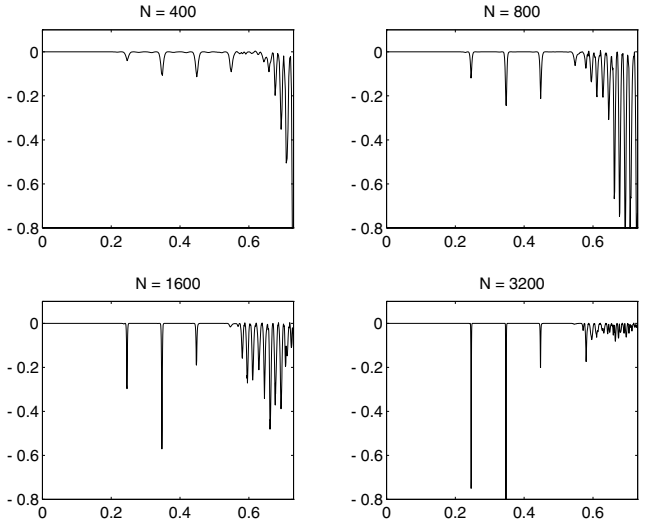

Fig. 2. NT scheme: entropy behind the main shock, $x \in [0, 0.73]$.

3.1. Entropy Production on a Smooth Transition

We first study the solution right behind the main shock, for values of $x \in (0.5, 0.7)$. We see that in this region, the NT scheme begins to show details of the "*exact*" solution around $N = 800$. The numerical solution seems to converge faster immediately behind the shock, and, for $N = 3200$, the numerical and the "*exact*" solutions are very close. We now consider the behaviour of the numerical entropy, see Fig. 2, which, in this region of the flow, should converge to zero. The entropy dissipation is small, when the numerical solution resolves well the details of the "*exact*" solution, and beyond that point it converges to zero fast, in the interval we are considering. Figure 3 shows both the local error and the entropy production for the

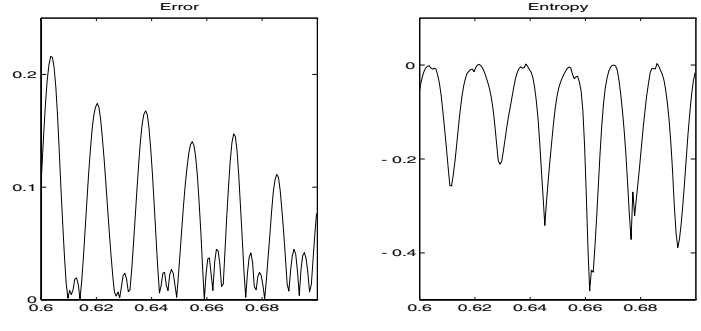

Fig. 3. NT scheme with $N = 1600$. Left: error with respect to the "*exact*" solution, for $x \in [0.6, 0.7]$. Right: entropy production.

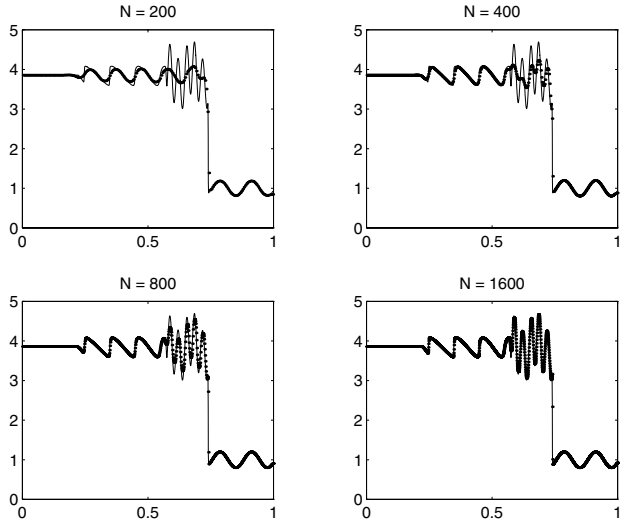

Fig. 4. C-CW3 scheme: density; $\lambda = \frac{3}{7}c$.

Nessyahu–Tadmor scheme on the $N = 1600$ grid in the region of smoothness behind the main shock. We note that both quantities have a similar behaviour and are of the same order of magnitude.

As soon as the local error becomes small, the spurious entropy production decays for all schemes we are considering. The rate of decay is

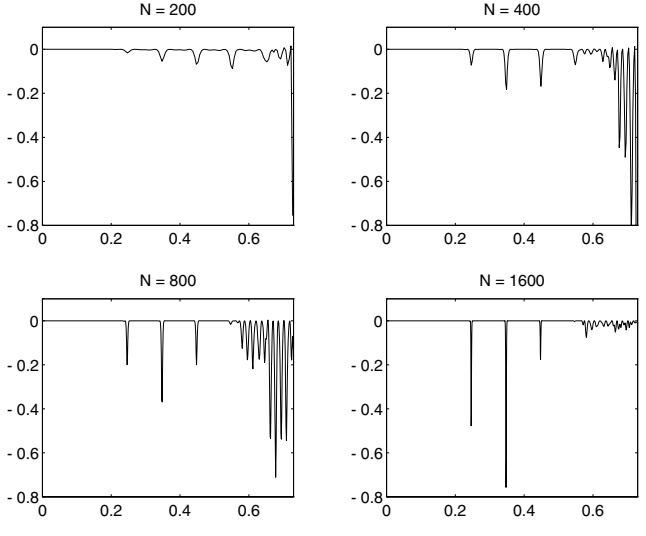

Fig. 5. C-CW3 scheme: entropy behind the main shock, $x \in [0, 0.73]$.

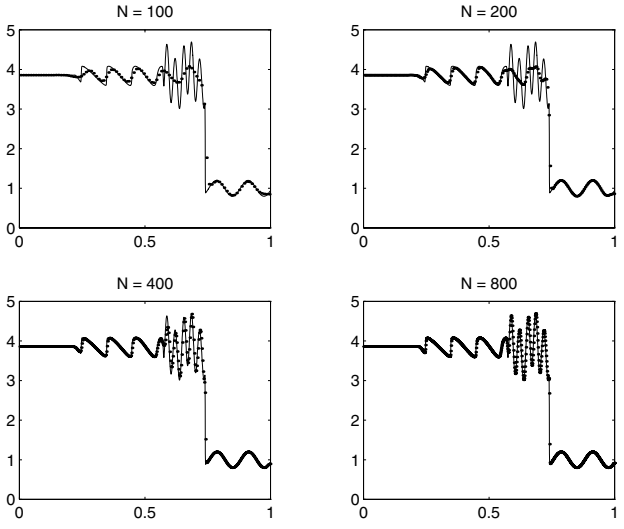

Fig. 6. CW4 scheme: density; $\lambda = \frac{2}{7}c$.

much faster for the more accurate C-CW3 scheme, and even faster for the CW4 scheme. This behaviour is very clear in Figs. 5 and 7, and it shows that these high order schemes maintain their high convergence rate, even behind the strong shock.

Thus we see that in the region of smooth flow immediately behind the main shock, the density of entropy production mimics the behaviour of the local error: a high spurious entropy production suggests the need for grid refinement when the "*exact*" solution is still underresolved. However, if the grid is so coarse that the numerical solution has no similarity with the "*exact*" solution, (see for instance the plot corresponding to the C-CW3 scheme with $N = 200$ in Fig. 4), the corresponding numerical entropy production can be deceptively small.

3.2. Entropy Production on Shocks

For all schemes studied in this work, the entropy plots show that the density of entropy production on shocks has a similar behaviour. The peaks in the entropy production approximately double as the grid is refined. This phenomenon was already noted in [5] for the scalar case and for shock tube problems, and it permits to single out shocks in the numerical solution. We see therefore that even in the case of systems of equations, the presence of shocks is characterized by sharp peaks in the entropy production, with amplitude proportional to $\frac{1}{h}$.

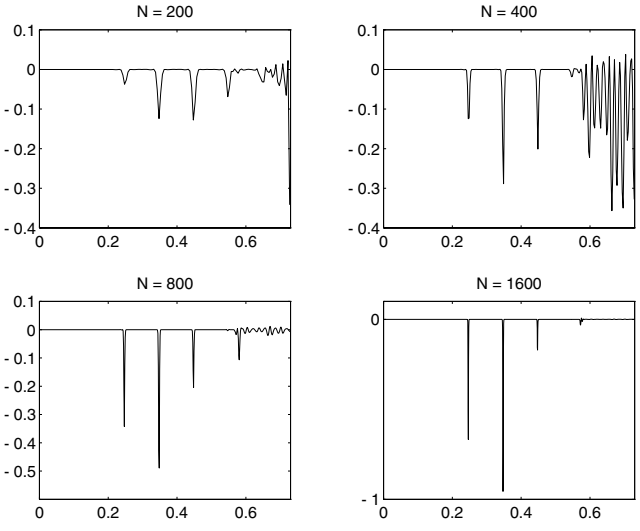

Fig. 7. CW4 scheme: entropy behind the main shock, $x \in [0, 0.73]$.

Note the different behaviour of the third peak in the entropy production, approximately located in the interval (0.4, 0.5). As the grid is fine enough to resolve this wave, the entropy diminishes under grid refinement, thus distinguishing this transition from the other shock waves.

REFERENCES

1. Godlewski, E., and Raviart, P.-A. (1996). *Numerical Approximation of Hyperbolic Systems of Conservation Laws*, Springer, New York.
2. Levy, D., Puppo, G., and Russo, G. (1999). Central WENO schemes for hyperbolic systems of conservation laws. *Math. Model. Numer. Anal.* **33**(3), 547–571.
3. Levy, D., Puppo, G., and Russo, G. (2000). Compact central WENO schemes for multidimensional conservation laws. *SIAM J. Sci. Comp.* **22**(2), 656–672.
4. Nessyahu, H., and Tadmor, E. (1990). Non-oscillatory central differencing for hyperbolic conservation laws. *J. Comput. Phys.* **87**(2), 408–463.
5. Puppo, G., *Numerical Entropy Production for Central Schemes*. Submitted to SISC.
6. Shu, C. W., and Osher, S. (1988). Efficient implementation of essentially non-oscillatory shock capturing schemes. *J. Comput. Phys.* **77**, 439–471.